National Library of Canada
Bibliothèque nationale du Canada

Canadian Theses Service
Service des thèses canadiennes

Ottawa, Canada
K1A 0N4

NOTICE

The quality of this microform is heavily dependent upon the quality of the original thesis submitted for microfilming. Every effort has been made to ensure the highest quality of reproduction possible.

If pages are missing, contact the university which granted the degree.

Some pages may have indistinct print especially if the original pages were typed with a poor typewriter ribbon or if the university sent us an inferior photocopy.

Reproduction in full or in part of this microform is governed by the Canadian Copyright Act, R.S.C. 1970, c. C-30, and subsequent amendments.

AVIS

La qualité de cette microforme dépend grandement de la qualité de la thèse soumise au microfilmage. Nous avons tout fait pour assurer une qualité supérieure de reproduction.

S'il manque des pages, veuillez communiquer avec l'université qui a conféré le grade.

La qualité d'impression de certaines pages peut laisser à désirer, surtout si les pages originales ont été dactylographiées à l'aide d'un ruban usé ou si l'université nous a fait parvenir une photocopie de qualité inférieure.

La reproduction, même partielle, de cette microforme est soumise à la Loi canadienne sur le droit d'auteur, SRC 1970, c. C-30, et ses amendements subséquents.

NL-339 (r. 88/04) c

Canada

An Ultrahigh Vacuum System for the Scattering of keV Ions by a Clean Si(100) Surface

by

Michel Jean Bruyère

Thesis submitted to
the School of Graduate Studies and Research
in partial fulfillment of the requirements for the degree
of Master of Science in Physics

Physics Department
Faculty of Science
University of Ottawa
Ottawa, Canada

Michel Jean Bruyère, Ottawa, Canada, 1990

National Library of Canada
Bibliothèque nationale du Canada

Canadian Theses Service
Service des thèses canadiennes

Ottawa, Canada
K1A 0N4

The author has granted an irrevocable non-exclusive licence allowing the National Library of Canada to reproduce, loan, distribute or sell copies of his/her thesis by any means and in any form or format, making this thesis available to interested persons.

L'auteur a accordé une licence irrévocable et non exclusive permettant à la Bibliothèque nationale du Canada de reproduire, prêter, distribuer ou vendre des copies de sa thèse de quelque manière et sous quelque forme que ce soit pour mettre des exemplaires de cette thèse à la disposition des personnes intéressées.

The author retains ownership of the copyright in his/her thesis. Neither the thesis nor substantial extracts from it may be printed or otherwise reproduced without his/her permission.

L'auteur conserve la propriété du droit d'auteur qui protège sa thèse. Ni la thèse ni des extraits substantiels de celle-ci ne doivent être imprimés ou autrement reproduits sans son autorisation.

ISBN 0-315-60024-1

Canadä

UNIVERSITÉ D'OTTAWA
UNIVERSITY OF OTTAWA

Abstract

An ultrahigh vacuum surface physics system was designed and built to study ion-surface interactions at various incident angles by detection of the forward scattered particles.

The proposed initial measurement is the scattering of keV ions by a clean Si(100) surface.

Résumé

Un système fonctionnant sous vide très élevé a été développé afin d'étudier la diffusion angulaire dans l'hémisphère antérieur d'ions défléchis sur une surface.

La première application suggérée de ce montage est à l'étude de la diffusion d'ions de quelques keV sur une surface (100) de silicium comportant très peu d'impuretés.

Acknowledgements

I would like to thank Dr. Brian Hird for the opportunity to work on a truly interesting experimental project and for the guidance and support he provided during my two-year term at the University of Ottawa.

I would also like to thank the entire staff of the Physics Department for making my stay a most enjoyable one.

I am very grateful to the Quebec F.C.A.R. Fund for a scholarship that enabled the completion of a M.Sc. degree without financial worries.

Finally, I would like to express my deep appreciation to my parents and family, whose backing and encouragement made this thesis possible.

Contents

Abstract		ii
Résumé		iii
Acknowledgements		iv
List of Figures		vi
Chapter 1	Introduction	1
Chapter 2	Ion Beam and Pressure Requirements	3
	2.1 Ion Production	3
	2.2 Ion Transport	8
	2.3 Vacuum Production	13
	2.4 Apertures	22
Chapter 3	Surface Considerations	26
	3.1 Surface Preparation	26
	3.2 Surface Position	33
Chapter 4	Scattered Ion Detection	35
	4.1 Geometry	35
	4.2 Rotating Platform, Racetrack and Arm	37
	4.3 Deflectors	40
	4.4 Detectors	46
Chapter 5	Proposed Measurement	49
Chapter 6	Conclusion	55
References		57

List of Figures

2.1	Arc Discharge Ion Source Danfysik 911A	4
2.2	Radio Frequency Ion Source	6
2.3	Ion Transport Overview	9
2.4	Mass Calibration Graph	11
2.5	Vacuum System Overview	14
2.6	Aperture Location	23
2.7	Aperture #2 and Anti-Scattering Aperture Assembly	24
3.1	Electron Beam Heater Mounted on Two-Rotation-Axes Sample Holder	28
3.2	Electron Beam Heater Power Supply	29
3.3	Temperature Controller On/Off Ratio	31
4.1	Scattered Ion Detection Geometry	36
4.2	Rotating Platform Assembly	38
4.3	Deflectors	41
4.4	Deflection Parameters	43
4.5	Channeltron Location	47
4.6	Pulse Counting System	48
5.1	Complete Measurement System	50
5.2	Voltage Divider Circuit	51
5.3	Example of Resulting Graphs	53
5.4	Definition of the Scattering Angle	54

CHAPTER 1 Introduction

The scattering of ions at surfaces is a well established field of physics. In many cases it is studied to elucidate the structure of the surface involved. It is also studied to detect effects related to the charge transfer occurring at the surface.

A surface physics system was designed and built[1] to study ion-surface interactions at various incident angles by detection of the forward scattered particles.

In the present work the apparatus that will allow the detection of both the neutral and ionic products of the scattering process is presented. The requirements for such an ion scattering experiment are:

- an ion source/accelerator system that produces ions of the desired energy (1 to 10 keV) in sufficient fluxes (10^{-6} A),
- a beamline with capabilities for steering, focusing and mass selection,
- a surface sample holder with capabilities for heating the sample, X,Y and Z translational movements, rotation about the principal axis, and rotation in a plane perpendicular to the principal axis (azimuthal rotation),
- deflecting electrodes for the analysis of the scattered particles,
- detectors that are sensitive to the scattered particles,

- electronics for amplifying, displaying and plotting the detected signals,

- an ultrahigh vacuum chamber to ensure sample cleanliness and differential pumping in order to keep the ion source/accelerator gas out of the chamber.

The present surface physics system fulfills these requirements. Its components are descibed in the following pages.

Silicon(100) was chosen as the first surface to be studied because it is easily cleaned and readily available.

The proposed measurement is to obtain graphs of the (ion counting rate)/(atom counting rate) ratio versus energy at various scattering angles and to combine these graphs in topographical plots of scattering angle versus energy where the contour lines would represent a constant counting rate ratio.

CHAPTER 2 Ion Beam and Pressure Requirements

2.1 Ion Production

Ion beams of only a small intensity (10^3 particles/sec) are needed for surface scattering measurements. However the requirements of the vacuum are such that the ions must pass through well spaced apertures, so that only a small acceptance solid angle of the ions from the source can be used. In practice this means that ion sources capable of emitting microamp beams into 10^{-6} Torr vacuum are required. Two types of ion sources are compatible with the surface physics system: the arc discharge ion source and the radio frequency (R.F.) ion source.

The arc discharge ion source is a hot filament, hollow cathode source (figure 2.1). In this type of source the arc discharge is very intense over a small volume and is optimized by surrounding it by the cathode, which is a helical tungsten filament placed between tantalum electrodes. A low pressure gas flows through a thermal mechanical leak into the cathode cavity. A high current (20-30 A) heats the filament, and electrons are thermionically emitted from the cathode to ionize the gas. A low voltage arc discharge is produced between the cathode and a tungsten anode. The arc is stabilized by controlling

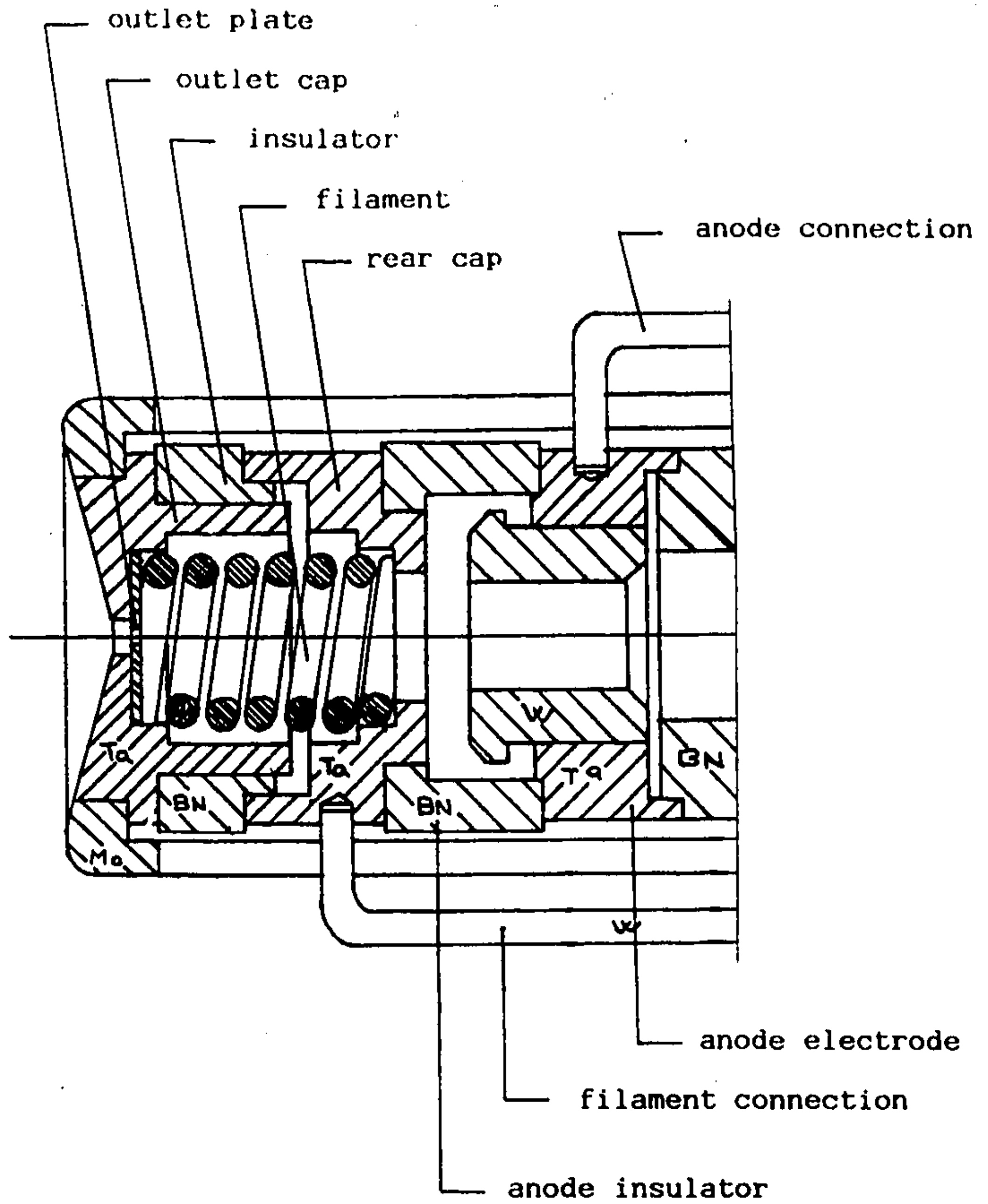

scale: 5:1

Figure 2.1

Arc Discharge Ion Source Danfysik 911A

the filament current and by using a high impedance arc power supply. Positive ions are extracted through a small pin-hole exit aperture on the opposite side to the anode. The arc discharge ion source used in the system is a commercially made Danfysik model 911A.

In the R.F. type ion source the discharge is produced inside a glass tube by external electrodes which are coupled to a high frequency oscillator (figure 2.2). The same gas supply system is used as in the hollow cathode source. Sufficient R.F. power is needed to fill most of the volume with plasma. A positive anode, in this case a wire, is sealed through the glass tube. The only other conducting material which is exposed to the plasma is a hollow metal tube, usually called the exit canal. Ions from the positively biased plasma are accelerated towards it and some escape into a much lower pressure region where they are extracted by a strong electric field.

Both types of ion source can produce beams of various elements of the periodic table but the arc discharge source is designed so as to yield a wider range of possible ions. The arc discharge type also has a better overall efficiency than the R.F. type: it produces more intense ion beams for a given input power. However it is a fragile source in which the filament breaks easily and a number of other problems occur on a regular basis. The R.F. source is not as

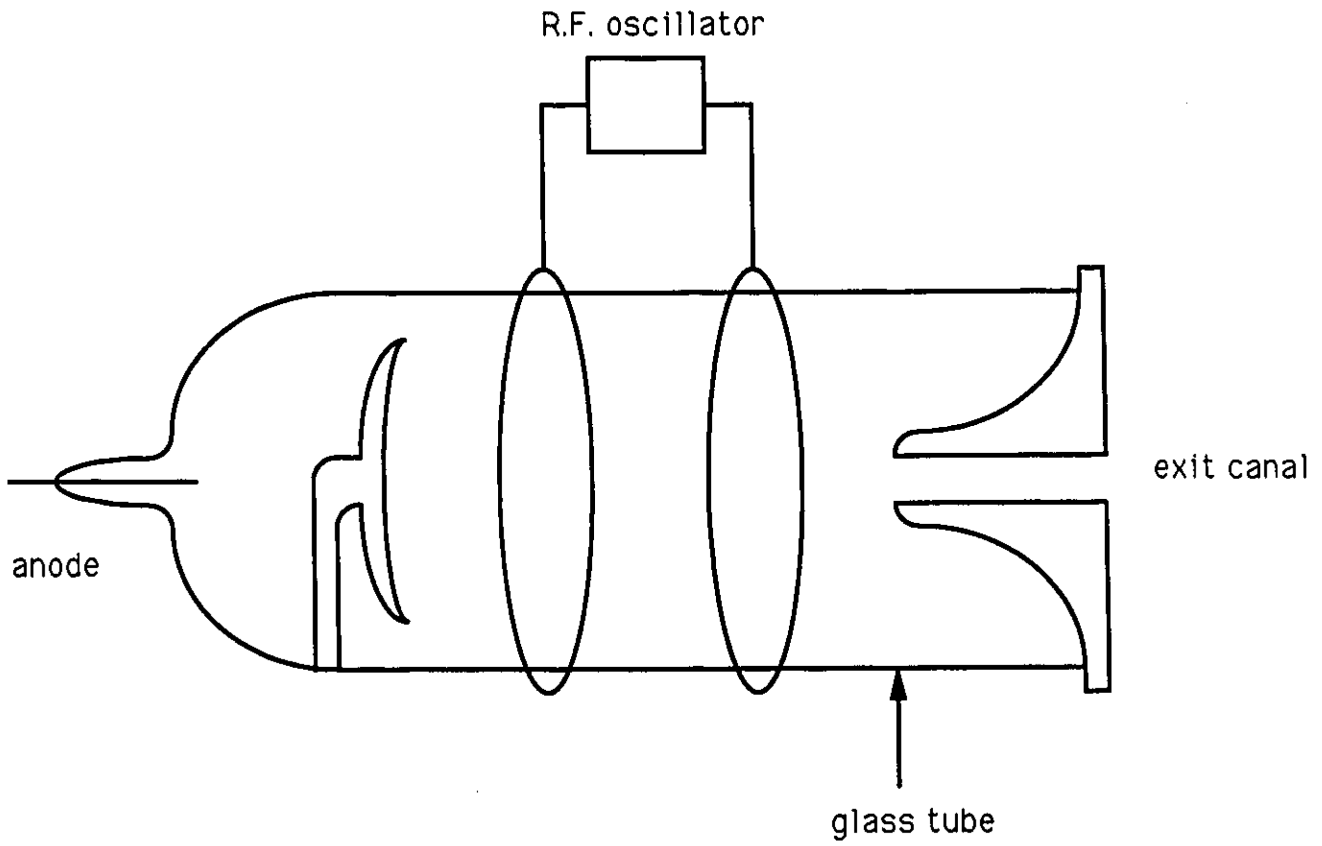

Figure 2.2

Radio Frequency Ion Source

delicate. Its design is simpler and more robust, although the glass discharge tube must be handled with care. The R.F. type is more versatile in the sense that it can produce both positive and negative ion beams.

2.2 Ion Transport

The ion beam is formed and transported using electric and magnetic fields (figure 2.3). An axial-tube electrode extracts the ions from the source. Inside the tube the ions are in a nearly field-free region before emerging into the roughly uniform electric field of the accelerator column. The fringe field between these two regions provides focusing so that the beam can be converged to a small diameter beyond the accelerator. The voltage of the accelerator ranges from 0 to 150 kV.

The accelerated ions are deflected toward the differential and main chamber sections by a 30° angle bending magnet. The magnet has the ability to separate out different ion masses by bending each mass at a different radius of curvature. A simple relation is obtained, first by considering the forces involved:

$$\frac{mv^2}{r} = qvB \tag{1}$$

where m, q and v are respectively the ion mass, electric charge and velocity, r is the radius of curvature and B the magnetic field. The ion velocity can easily be expressed as a function of the accelerating voltage V:

$$E = qV = \tfrac{1}{2}mv^2 \tag{2}$$

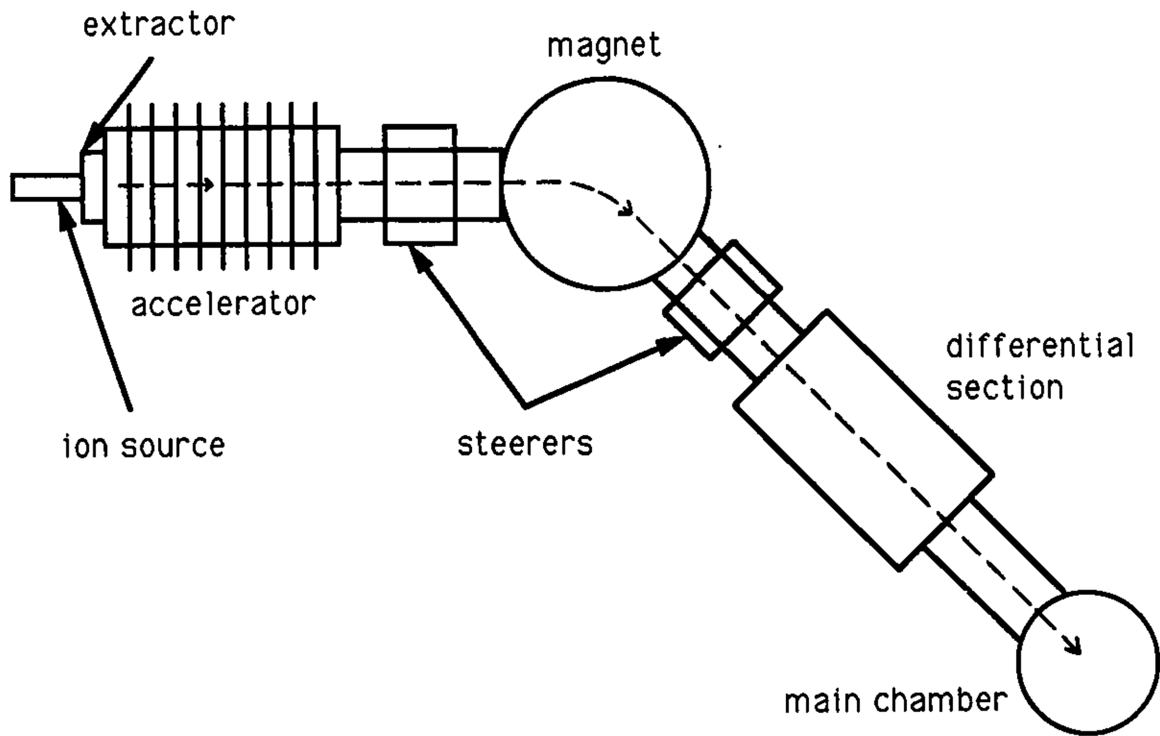

Figure 2.3

Ion Transport Overview

thus

$$v = \sqrt{\frac{2qV}{m}} \quad . \tag{3}$$

Combining equations (1) and (3) and rearranging we obtain

$$\frac{mV}{q} = \frac{r^2 B^2}{2} \quad . \tag{4}$$

The mass spectrum of the ions is determined by measuring the beam current which passes through a small fixed aperture as a function of the magnet current. Thus r is constant and we have

$$m \propto \frac{qB^2}{V} \tag{5}$$

for all ions of mass m and charge q which pass through the aperture.

All ion mass/charge ratios m/q should lie on the same straight line of a graphical plot of $\frac{mV}{q}$ as a function of B^2 for all values of accelerating voltage V. This line was established using a pure, well known, ion mass (argon gas in the ion source) at many accelerating voltages, and then the masses of other atomic and molecular impurity ions could be determined by interpolation (figure 2.4).

In practice the current I through the magnet is used as a measure of B, and hysteresis effects are minimized by always scanning in one direction.

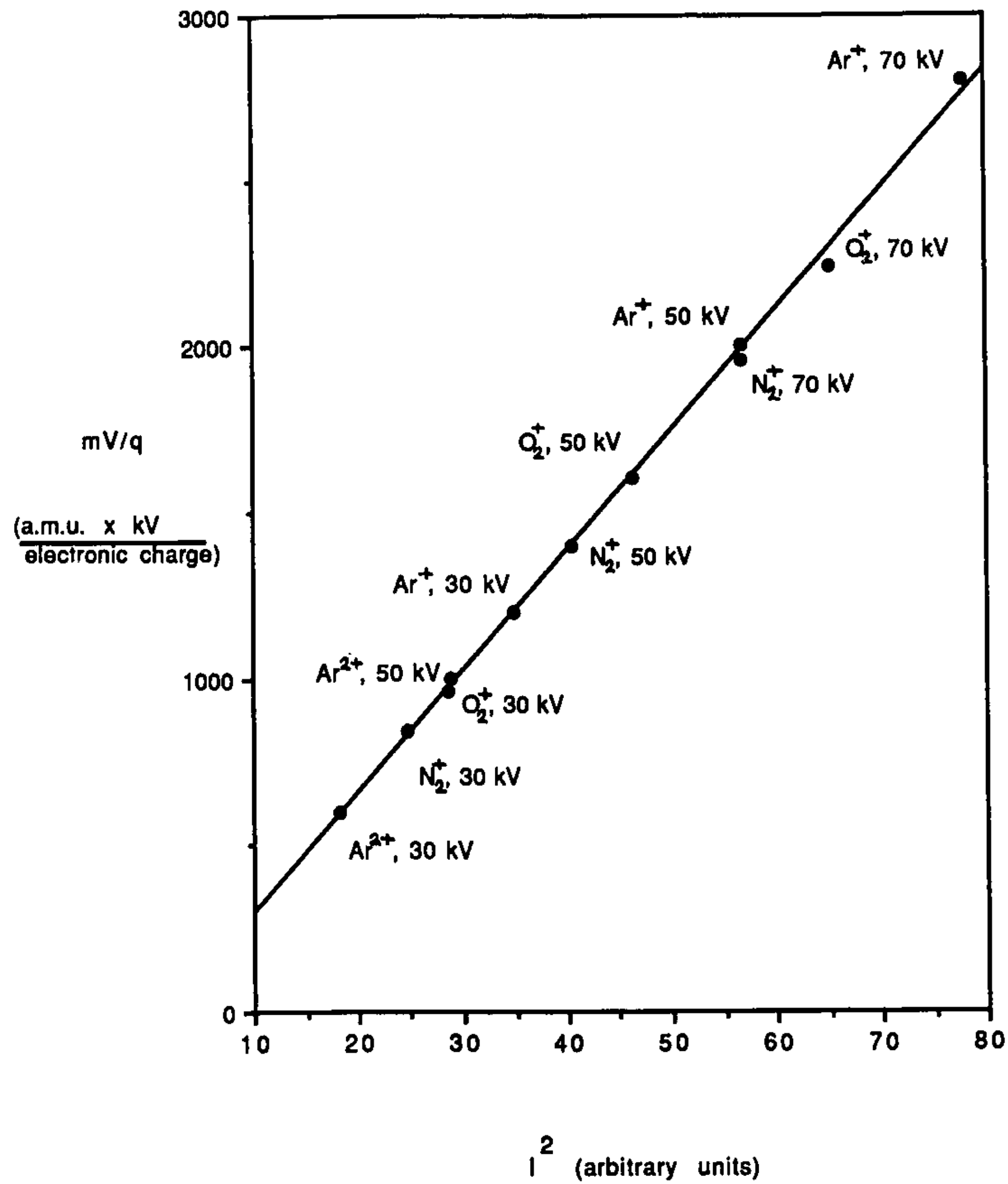

Figure 2.4

Mass Calibration Graph

The beam is guided through the system using two magnetic steerers, one on each side of the bending magnet. A steerer consists of four coils, wound around a square iron core, which surrounds the beam line. The coils on opposite sides are connected in series, in such a sense that their fields are opposed inside the iron. The return fields thus emerge from the iron and produce a weak, nearly uniform field in the vacuum. Fields of a few hundred gauss over a 20 cm length of the ion beam are sufficient to produce deflections of a few degrees. Because the fields are weak there is little iron saturation and the current/field relation is nearly linear. Consequently the left/right deflection, which is determined by the magnitude and direction of the current in the top and bottom coils in series, is substantially independent of the current in the left and right coils in series, which controls the up/down deflection, and vice versa.

2.3 Vacuum Production

The vacuum system can be divided in three components (figure 2.5):

- the accelerator section,
- the differential section,
- the main chamber section.

A 10^{-6} Torr pressure is maintained in the accelerator section by two 100 l/s diffusion pumps backed by a common rotary pump. A first aperture separates this accelerator section from the differential section. A gate valve is also included to fully isolate these two sections when needed.

The middle component of the vacuum system, the differential section, serves as a vacuum buffer between the "dirty" 10^{-6} Torr accelerator section and the ultrahigh vacuum main chamber. The section consists of a long straight pipe and a four-way cross, both of 150 mm inside diameter. Its total length is 733 mm. The differential section is pumped by a 200 l/s UHV diffusion pump/cold trap system which is a smaller version of that used for the main chamber. A second aperture and a straight-through all-metal valve separate the differential section from the main chamber section.

The main chamber can be pumped down to 10^{-10} Torr by a 415 l/s diffusion pump/cold trap system backed by the same

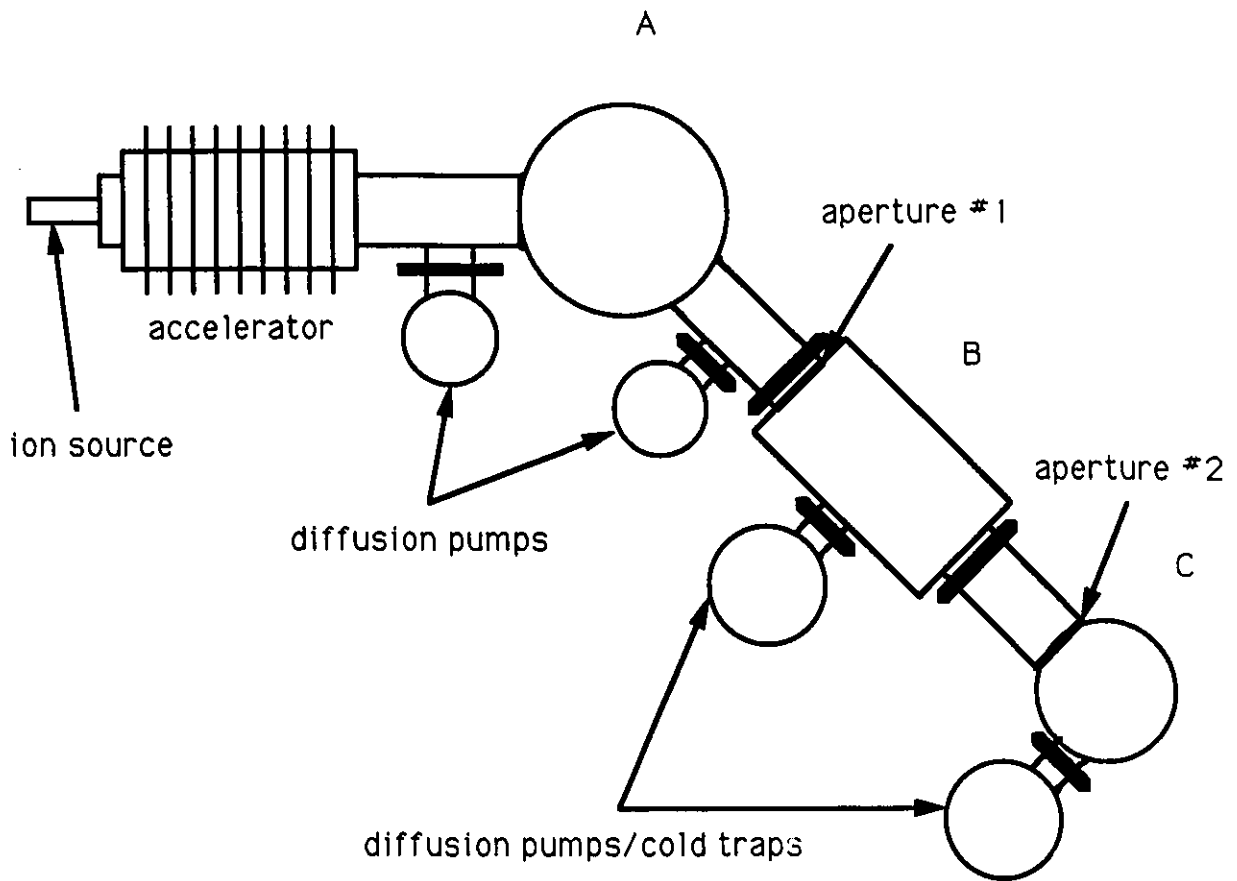

▬ : valve
A : accelerator section
B : differential section
C : main chamber section

Figure 2.5

Vacuum System Overview

rotary pump as the differential section. The chamber is a 508 mm-high stainless steel cylinder with an inside diameter of 293 mm and an outside diameter of 305 mm. It has twenty-seven ports of several different diameter sizes, two of which have Pyrex windows of 100 mm and 150 mm respectively.

The accelerator section has a conventional vacuum technology system so that O-rings are used everywhere. The differential and main chamber sections require UHV techniques which use a bakeable system, so that all seals are copper gaskets compressed between the knife edges of two stainless steel Conflat flanges. The exception is an internal large diameter poppet valve, to isolate each pump from the system, which uses a Viton O-ring seal. Viton is a special high temperature elastomer with a much lower outgassing rate than nitrile rubber. The use of Viton O-rings is allowable for UHV, but they must be prebaked and they can only be used to separate different sections of vacuum. The Viton seals limit the maximum baking temperature to 300°C.

The main chamber is further equipped with a titanium sublimation pump to getter the outstanding contaminants. It is held in reserve to achieve the best possible vacuum prior to starting an experiment.

Several calculations were performed to determine if the pumping speeds of the diffusion pump/cold trap arrangements were sufficient to reach a pressure of 10^{-10} Torr in the main chamber. The gas flow rate through an orifice was deduced from the kinetic theory formula[2]

$$\text{flow rate} = \frac{1}{4} n\bar{v}A \qquad (6)$$

where n is the gas molecules density on the high pressure side of the orifice, $\bar{v}$ is the mean speed of the molecules (480 m/s at 20°C for air), and A is the area of the orifice. Equation (6) yields the flow rate in molecules/sec. Converted to volume flow rate, it becomes

$$\text{volume flow rate} = \frac{1}{4} \bar{v}A \qquad (7)$$

independent of pressure, where the volume flow is on the high pressure side. Assuming a circular orifice of diameter D we have

$$\text{volume flow rate} = \frac{1}{4} \bar{v} \frac{\pi D^2}{4} \qquad (8)$$

or approximately, when D is expressed in cm, and the flow rate is in l/s

$$\text{volume flow rate} = 3\pi D^2 \text{ l/s.} \qquad (9)$$

This relation is independent of the pressure on the high pressure side and neglects back flow from the low pressure

side. This result is used to calculate the gas flow through two spaced apertures of diameter $D = 2$ mm separating the three sections at pressures of 10^{-6}, 10^{-8} and 10^{-10} Torr respectively, a good approximation to the present vacuum system. The calculated flow rate on the high pressure side of both apertures is

$$\text{volume flow rate} = 3\pi(0.2)^2 \text{ l/s} = 0.38 \text{ l/s} . \qquad (10)$$

Since there is a 100:1 ratio of pressures between the two sides of each aperture, this flow rate becomes 38 l/s on the low pressure side of each aperture. This rate is safely below the pumping speed of 200 l/s for the differential section and 415 l/s for the main chamber.

There was also concern about the molecules which pass directly from the 10^{-6} Torr region into the 10^{-10} Torr region. The flow rate into a small solid angle $d\Omega$ is

$$\text{direct flow rate} = \text{total flow rate} \times \frac{d\Omega}{\pi} \qquad (11)$$

with the total flow rate being given by equation (9). The solid angle between the apertures, spaced by a distance L, is expressed by

$$d\Omega = \frac{\pi D^2}{4} \frac{1}{L^2} . \qquad (12)$$

Substituting equation (12) in equation (11):

$$\text{direct flow rate} = 3\pi D^2 \times \frac{\pi D^2}{4L^2} \times \frac{1}{\pi} \quad \text{l/s} \tag{13}$$

or

$$\text{direct flow rate} = \frac{3}{4}\,\pi\,\frac{D^4}{L^2} \;\; \text{l/s.} \tag{14}$$

The direct flow rate in the previously described vacuum system, using a value of $L = 1$ m for the spacing between apertures, is

$$\text{direct flow rate} = \frac{3}{4}\,\pi\,\frac{(0.2)^4}{(1)^2}\ \text{l/s} = 3.8 \times 10^{-3}\ \text{l/s.} \tag{15}$$

This direct flow rate of 3.8×10^{-3} l/s at 10^{-6} Torr becomes 38 l/s at 10^{-10} Torr (in the main chamber), which is the same as the molecular flow from the 10^{-8} Torr region. Thus we conclude that the two apertures must be well separated, with a distance of the order of 1 m between them, to prevent the direct flow from being important. The combined flow rate from both types of flow is well below the pumping speeds of the pumps.

Some reduction in the flow rate can be achieved by using a tube of finite length instead of a short aperture. The flow rate for a tube of length L is reduced by a factor $\frac{1}{1 + \frac{3}{4}\frac{D}{L}}$ compared to a zero length aperture of the same diameter[3].

An elaborate arrangement of pipes, bellows and valves is in place for roughing and backing the differential and main chamber sections. This system allows all possible options of roughing and/or backing of the two sections either jointly or independently, while minimizing mechanical vibrations. It includes an up-to-air valve.

Three ionization gauges, one in each section, allow the monitoring of the system pressure. Six strategically located thermocouple gauges measure the roughing and backing pressures.

Numerous precautions are taken to ensure the cleanliness of the differential and main chamber sections. It is of great importance to create the best environment possible for the preparation and maintenance of a clean surface sample. A bakeout oven is designed so that both sections can be baked at 200°C jointly or separately. Baking is necessary to reduce the surface outgassing in both ultrahigh vacuum sections and therefore improves vacuum conditions after cooling back to room temperature. Also, every piece of hardware in the system is made only of UHV compatible material: stainless steel, copper, gold, Pyrex, Viton, Teflon, Macor, sapphire, molybdenum, thoria, iridium, alumina, etc.

All components are cleaned with solvent (acetone then isopropanol) in an ultrasonic bath prior to their insertion

in the UHV main chamber. Solvent is also used to clean tools coming into contact with UHV components. Both tools and components are handled with plastic gloves. When the main chamber must be opened, filling it with nitrogen through the up-to-air valve reduces the amount of water vapour entering the chamber and facilitates the subsequent pump down. The raw concrete in the vicinity of the surface physics system and of the stored components is painted to reduce the amount of concrete dust. The components not being used are stored on a shelf-unit and on a table both covered with plastic sheets to protect from dirt. Finally, both rotary pumps are outfitted with oil mist filters.

Table 2.1 gives the values for the best pressure reached in each of the three sections of the surface physics system. The pressures of the differential and main chamber sections were reached when both cold traps were filled with liquid nitrogen. It is these special cold traps that enable the diffusion pump system to be useable to UHV. The performance of the traps is independent of the liquid nitrogen level, since the bulk of the condensate collects on chevrons, welded to the bottom of the reservoir, that do not warm up until all the liquid nitrogen has boiled off. Condensate evaporating from the reservoir as the level falls is re-condensed lower down on the reservoir because condensate molecules are unlikely to escape from the narrow

annular gap between the reservoir and trap body without colliding with the cold reservoir again. It is found that the system pressure is constant until the trap reservoir is empty, the pressure then steadily increasing. The best vacuum results were obtained after the diffusion pumps had been running for many days, the oil seemingly cleaning itself during continuous pumping. It was also discovered that the indium wire gasket used for sealing the diffusion pump/cold trap interface is reusable if handled with caution.

Table 2.1

Best Pressures Reached in Vacuum System

	Section		
	Accelerator	Differential	Main chamber
Best Pressure (Torr)	7.1×10^{-7}	5.5×10^{-10}	3.5×10^{-10}

2.4 Apertures

The three apertures of the surface physics system serve not only to reduce the gas load in the UHV section but also to collimate the ion beam (figure 2.6).

Aperture #1 separates the accelerator section from the differential section while aperture #2 separates the differential section from the UHV main chamber section. These two apertures are 1 m apart. Aperture #2 and the anti-scattering aperture are 5 cm apart.

All three apertures can be changed quite easily, especially aperture #2 and the anti-scattering aperture that are part of an assembly designed for that purpose (figure 2.7). These two slits are accessed through the 150 mm window of the main chamber. Any given aperture can be replaced with another aperture of a different diameter to modify the beam optics.

Both aperture #1 and aperture #2 are electrically isolated from the stainless steel beam line to allow the measurement of the current produced by the ion beam striking their surface. A pair of Keithley picoammeters measure the current. This feature is very helpful in the guidance of the beam and in the determination of the ion source output.

Early tests were made with two rectangular apertures of 2 mm x 4 mm at right angle from each other so as to explore

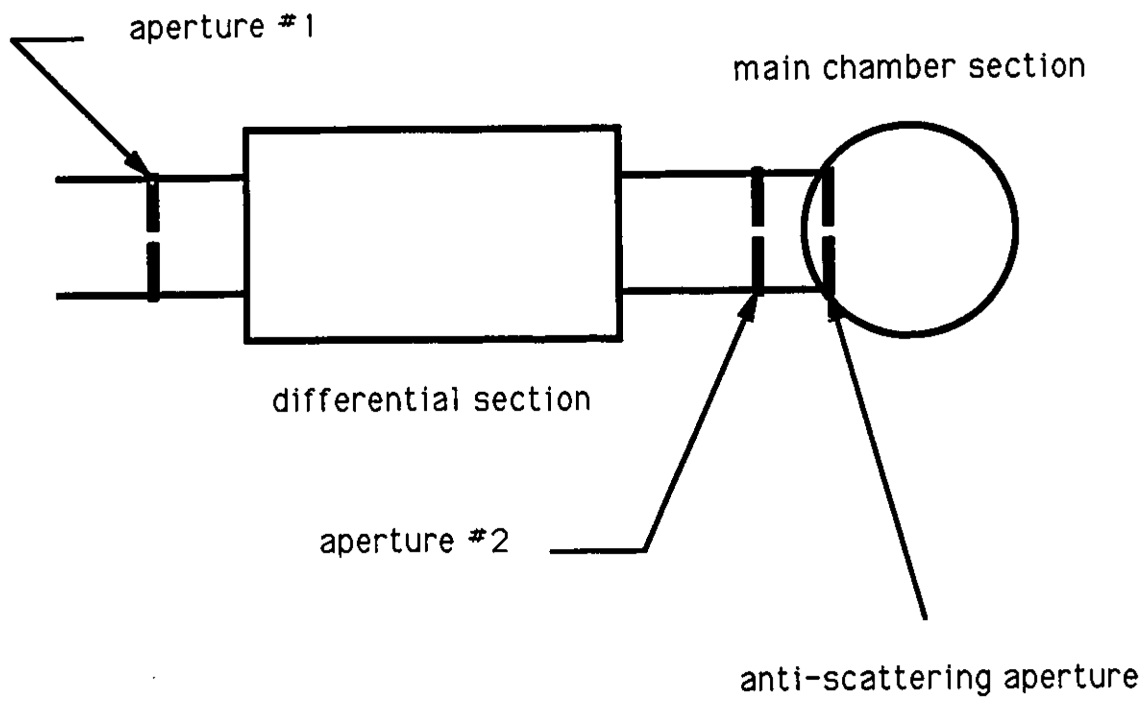

Figure 2.6

Aperture Location

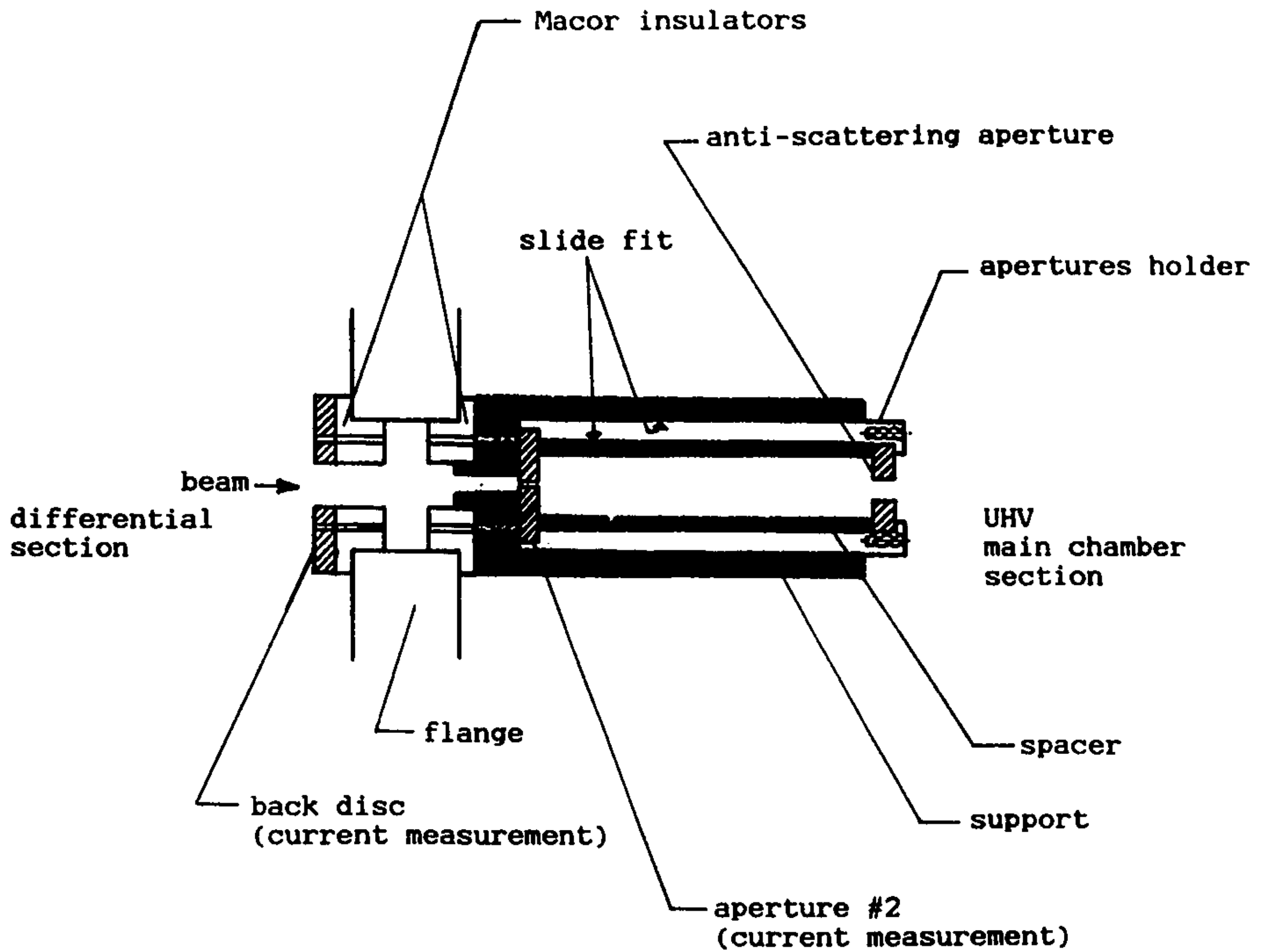

scale: 1:1

Figure 2.7

Aperture #2 and Anti-Scattering Aperture Assembly

the mechanical alignment of the system. In agreement with the design calculations, it was found that there was only slight variation of the pressure in the differential section when the accelerator section was connected. Later aperture #2 was reduced in size to diminish the beam intensity so that the design requirements of the gas flow into the UHV chamber were amply fulfilled.

Presently in the system, aperture #1 is a rectangular vertical slit of 2 mm x 4 mm, and aperture #2 is a tiny circular opening of diameter 0.009".

CHAPTER 3 Surface Considerations

3.1 Surface Preparation

The first surface to be studied with the system will be silicon(100). Wafers were provided by both the National Research Council and Bell-Northern Research. The wafer diameter is 3" and the thickness about 380 μm. Rectangular samples of 15 mm X 12 mm are cut from a wafer using diamond marking pencils. The cutting procedure is to rest the wafer on lens cleaning tissue which is a conveniently soft, clean and lint-free medium. A diamond point is pressed onto the surface and, on the opposite side of the wafer, along a cleavage line, another diamond point scratches the edge of the wafer until it cracks along the line between the two diamond points. In this way rectangular pieces of any size are easy to produce.

The cut surface sample is handled with special Teflon tweezers. It is installed in the UHV main chamber on the specimen attachment module of the manipulator system (see next section). The surface sample is firmly held in place by a pair of molybdenum spring clips. The replacement of the sample is made through the 150 mm window, or by removing the manipulator.

The attachment module is equipped with an electron beam heating accessory (figure 3.1). To ensure a clean surface the sample will be heated to 1000°C in ultrahigh vacuum immediately before the start of an experiment.

A power supply (figure 3.2) was designed and constructed to provide the necessary heating. The type of heating used is described as electron beam heating. The filament is located directly behind the sample backplate which also acts as a grounded anode. A temperature of 500°C can be reached by thermal radiation from the hot filament only. More intense heating of up to 1200°C is achieved by applying a high negative voltage to the filament, so that the backplate becomes the anode of a thermionic diode and is heated by the electron beam. A power supply of 600 V/100 mA DC is used for this purpose.

Heating at a selected temperature is realized by means of a sophisticated temperature controller that senses the sample temperature with a NiCr/NiAl thermocouple mounted under one of the molybdenum spring clips. A second thermocouple under the opposite clip can be used as an independent monitor. According to the measured and selected temperatures, the temperature controller activates or deactivates a solid state relay in series with the filament power supply. Because of the small thermal time constant of the filament, the ordinary commercial temperature

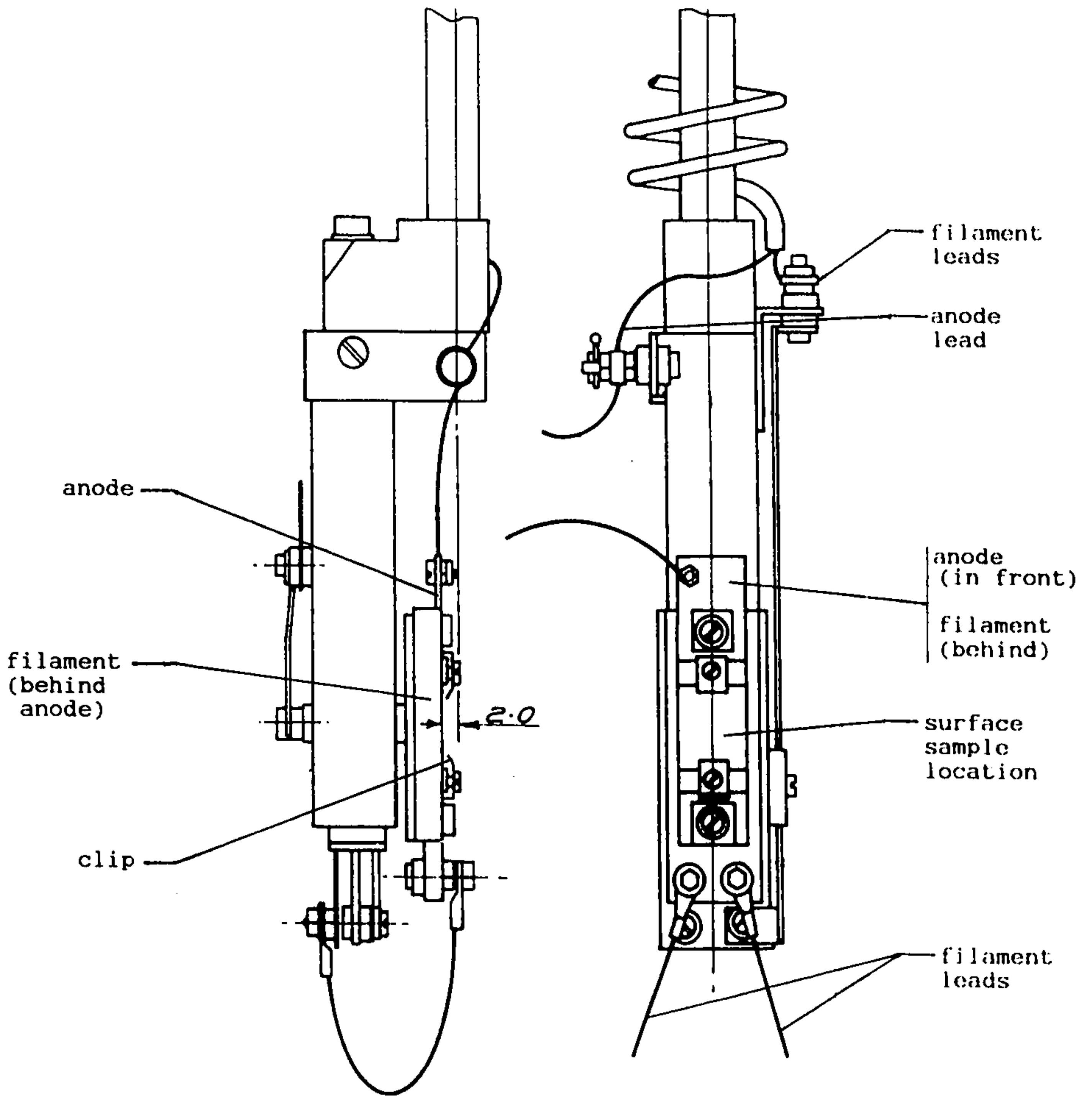

Figure 3.1

Electron Beam Heater
Mounted on Two-Rotation-Axes Sample Holder

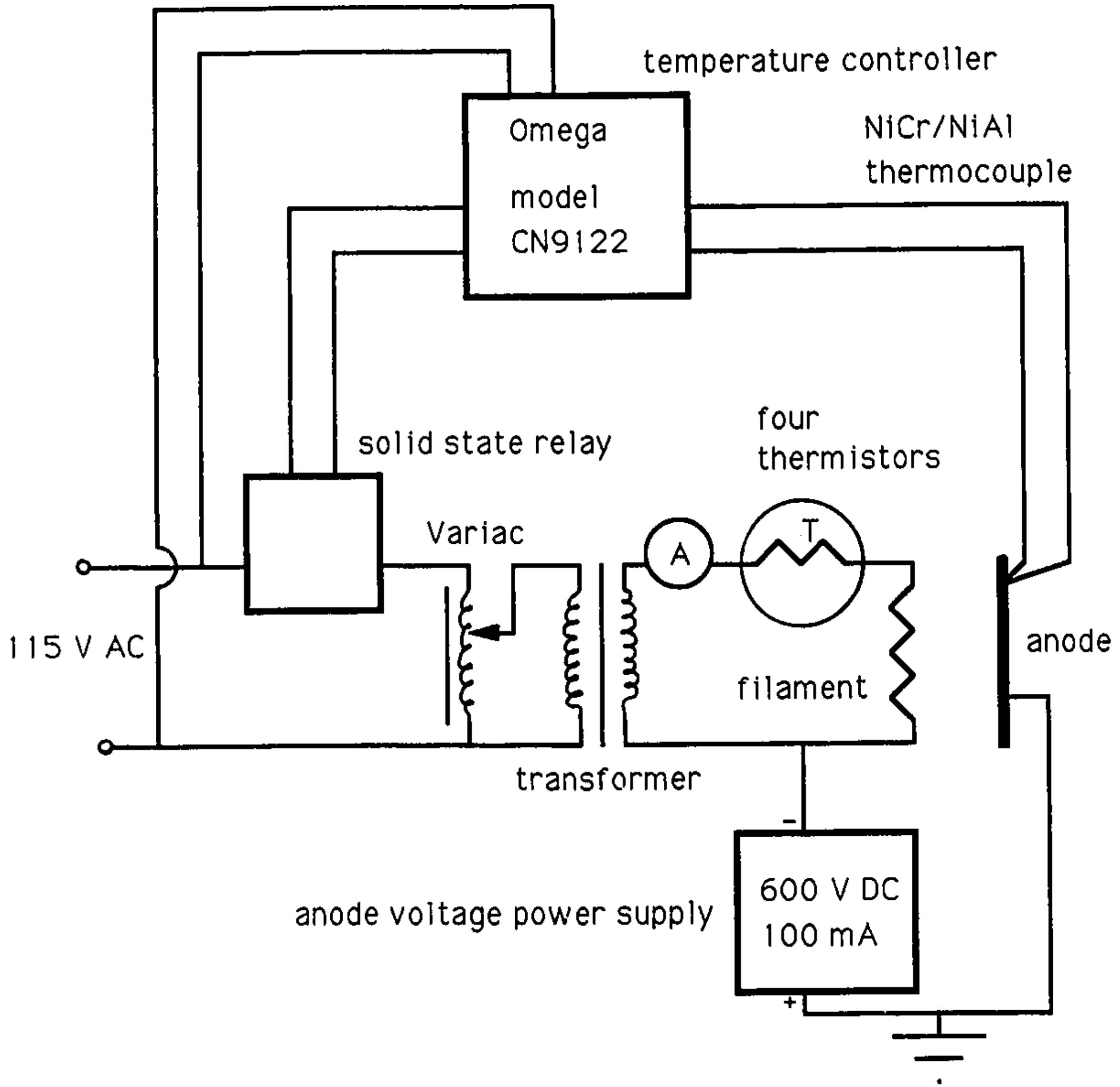

Figure 3.2

Electron Beam Heater Power Supply

controllers were unsuitable. Temperature controllers which were described as "proportional" were found in fact to switch the full current on/off completely, and it is the ratio of on/off times which was varied proportionally from 100% some degrees below to 0% very close to the set point (figure 3.3). A rapid cycling commercial type was finally found which would operate at 20 Hz. It is hoped that this is fast enough to smooth out the temperature oscillations on the silicon sample surface.

A Variac is included in the electron beam heater power supply circuit to reduce the thermal shock on the surface sample during both the initial starting up and final cooling down processes. It was also found there was a need to minimize the shock to the filament produced when the solid state relay is switched on and off. A small circuit was designed for that purpose. It consists of four thermistors connected in series, each with a cold resistance of 5 Ω and a hot resistance of 1 Ω. This simple device solved the thermal shock problem. An ammeter was added to display the filament current to ensure it is kept below the rated maximum of 2.1 A AC.

The electron beam heater was tested in the following manner. A temperature of 800°C was selected as the set point on the temperature controller. The Variac was slowly turned up from zero to increase the filament current, so that the

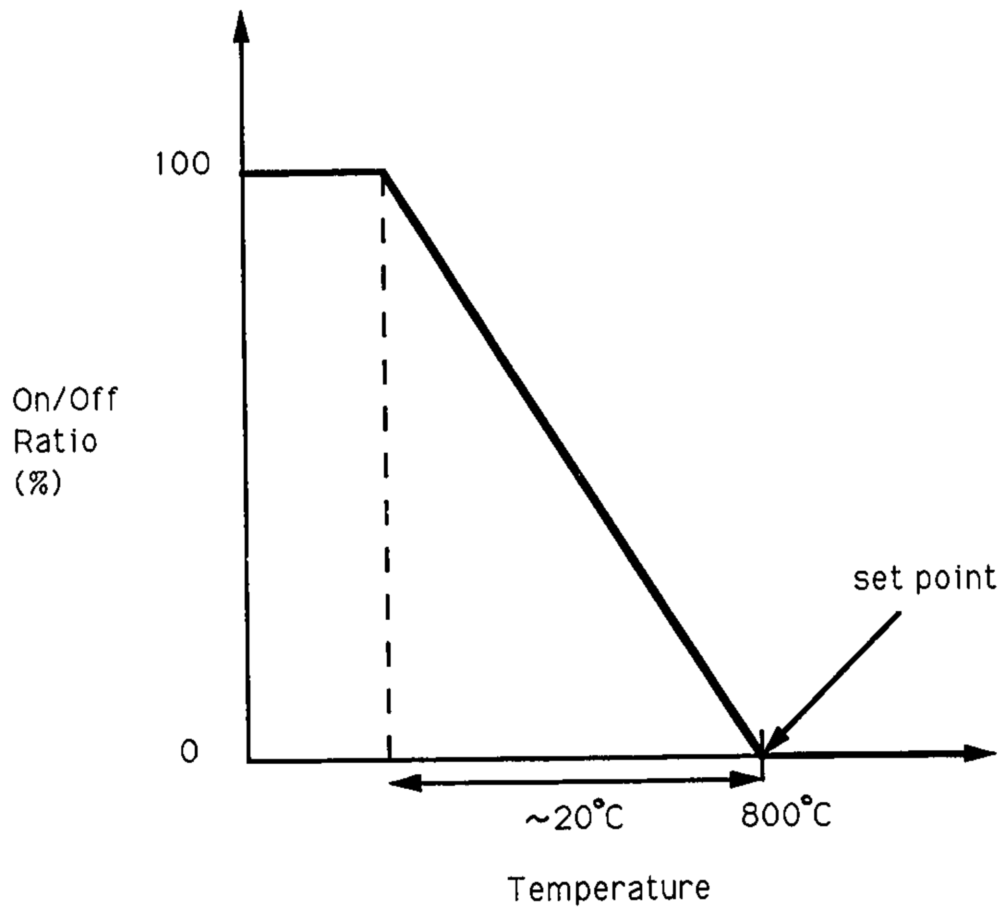

Figure 3.3

Temperature Controller On/Off Ratio

temperature rose slowly, until the current was about 1.5 A. The anode voltage was applied and along with the filament current it was carefully increased to slowly approach the set point. Near the set point the solid state relay began to cycle on/off. Fine tuning consisted in providing just enough power to maintain the on/off cycle with no excursion into the fully on or fully off regions. It usually stabilized quickly to this condition after a fine adjustment. Typical values for a heating temperature oscillating between 785°C and 798°C were 1.6 A of filament current and 350 V of anode voltage at 82 mA.

3.2 Surface Position

The surface sample is located at the centre of the ultrahigh vacuum main chamber, which is the focus of all the ports around the upper level of the chamber.

The sample hangs vertically downward on a commercially made manipulator mounted on the top flange of the UHV main chamber. The manipulator and sample holder in combination provide XYZ translation movements, and rotations about two perpendicular axes. The system thus possesses five degrees of freedom to accurately position the surface sample. The XYZ translator allows the sample to be accurately positioned in line with the incoming ion beam or to be moved out of the way. The manipulator carries a double rotary drive in which the primary drive gives a 0 to 360° rotation about a vertical axis. A secondary rotary drive moves an internal co-axial shaft in an upward/downward direction. This motion is converted to $\pm 90°$ rotation about a horizontal axis by means of a precision rack and pinion drive on which the sample holder is mounted.

The manipulator is a high precision device, bakeable to 230°C. The translational resolution of the manipulator is 0.005 mm for the X, Y and Z axes. The angular resolution is 0.1° on the primary rotation axis and 0.3° on the secondary axis.

The incident beam angle ϕ_i is selected with the primary rotation of the manipulator while the secondary rotary motion determines the alignment of the crystallographic directions of the surface sample.

CHAPTER 4 Scattered Ion Detection

4.1 Geometry

The surface sample is located at the centre of the main scattering chamber (figure 4.1). It is positioned about 13 cm downstream from the anti-scattering slit. The plane of scattering is horizontal, with the incident angle ϕ_i being determined by the vertical rotation axis of the specimen manipulator and the scattered angle ϕ being determined by the position of the detectors on the horizontal racetrack. The scattered ions are separated from the neutral atoms by a vertical electric field and both are counted with two channel electron multipliers (channeltrons), one vertically above the other. Thus the neutral atoms and charged ions which are scattered at the same angle are counted simultaneously.

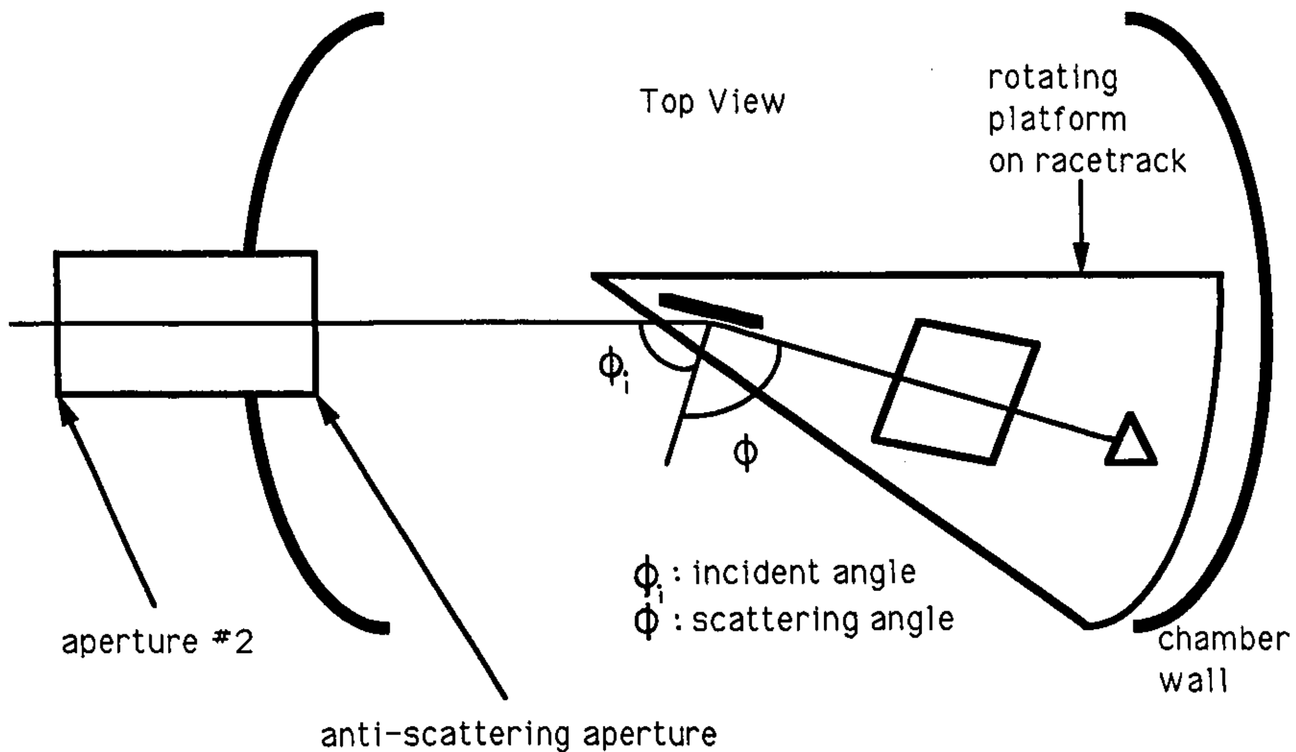

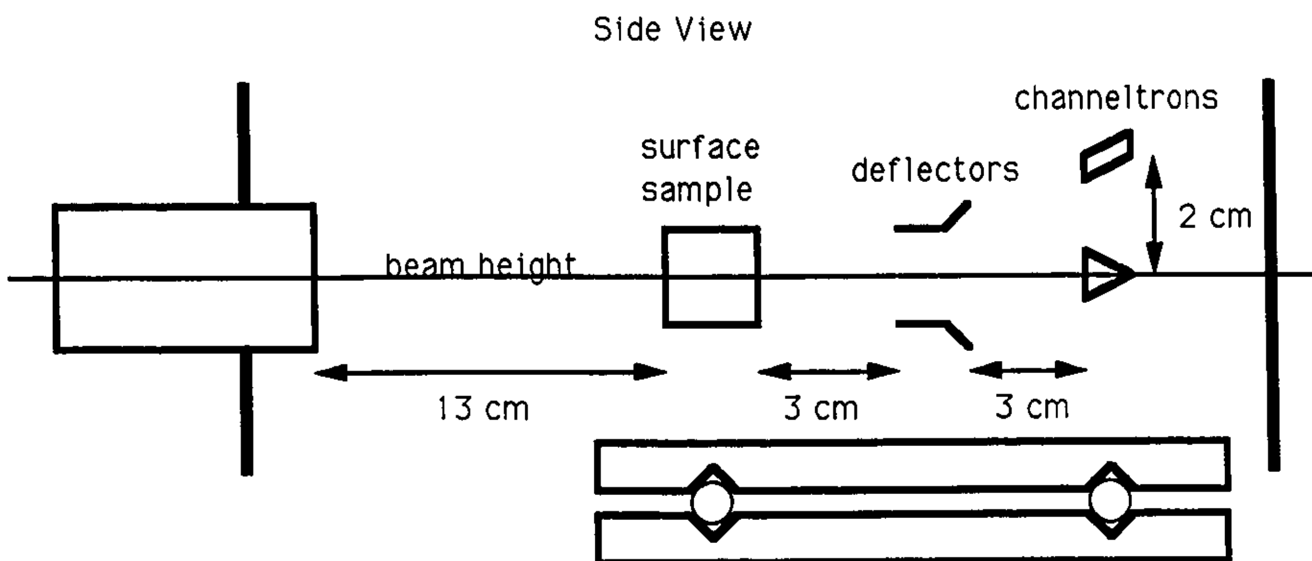

Figure 4.1

Scattered Ion Detection Geometry

4.2 Rotating Platform, Racetrack and Arm

The deflectors and detectors are mounted on a horizontally rotating platform assembly (figure 4.2) in order to allow an angular scan of the scattered ion beam. The platform also provides a means to move the detectors safely away from the ion beam path.

The rotating platform itself is a stainless steel pie-shaped wedge of 50° of arc. It rests on sixteen $\frac{3}{8}''$ stainless steel ball bearings along its arc and on a single ball bearing at the centre of rotation. The pivot coincides with the centre of the main chamber and with the vertical axis of the manipulator. The ball bearings are kept evenly spaced on a racetrack by a thin curved plate separator. The racetrack is simply a machined groove in a two-piece platform support designed so that it can be withdrawn through the 150 mm viewport. This stainless steel support rests on a tripod structure in the main chamber.

A flexible arm is used to move the rotating platform along the racetrack. It consists of three rigid segments and two flexible joints. One end of the arm is attached to the rotating detection platform and the other to a rotational motion feedthrough constructed from a bent bellows. A rotation of the feedthrough from outside the main chamber therefore results in a rotation of the detector platform

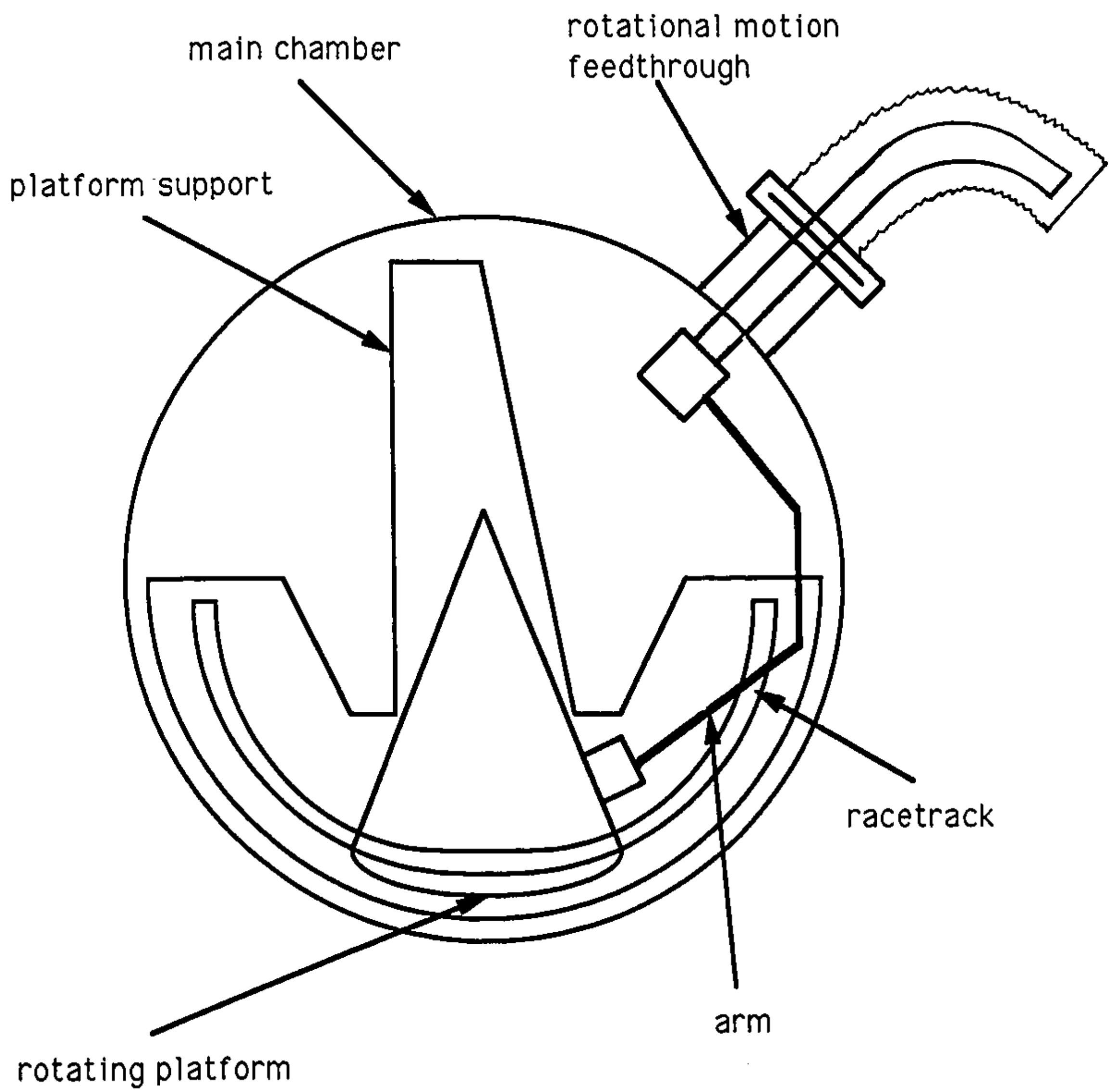

Figure 4.2

Rotating Platform Assembly

inside the chamber and allows the location of the detecting assembly at a desired angle. The platform is designed to be rotated up to 120° in the horizontal plane. But this range is limited by the flexibility and length of the arm as well as by the numerous copper wires in the neighborhood of the platform assembly.

4.3 Deflectors

The analysis of the particles scattered from the surface sample starts with a charge separation caused by the electric field between two electrodes (figure 4.3).

The deflection electrodes are 4 cm wide and 4 cm long. For half of that length the electrodes are parallel with a spacing of 1 cm, then they are bent away from each other so that the spacing at the exit is doubled to 2 cm. This tapered shape prevents ions from striking the electrodes while allowing the ions to be deflected to the top channeltron.

The deflectors are positioned at 3 cm from the sample on the scattering side at a height such that a straight-through beam is equidistant from each electrode.

The degree of deflection of a charged particle passing between a pair of electrodes is controlled by the potential difference V between those electrodes. For parallel electrodes the angle of deflection θ is related to the voltage V across the electrodes by the simple expression

$$\theta_{\mathrm{par.}} = \frac{q}{2E}\,\frac{l_0}{d_0}\,V \qquad (16)$$

where q is the electric charge of the ion and E its energy, l_0 is the length of the electrodes and d_0 the spacing between them. In the case of non-parallel straight

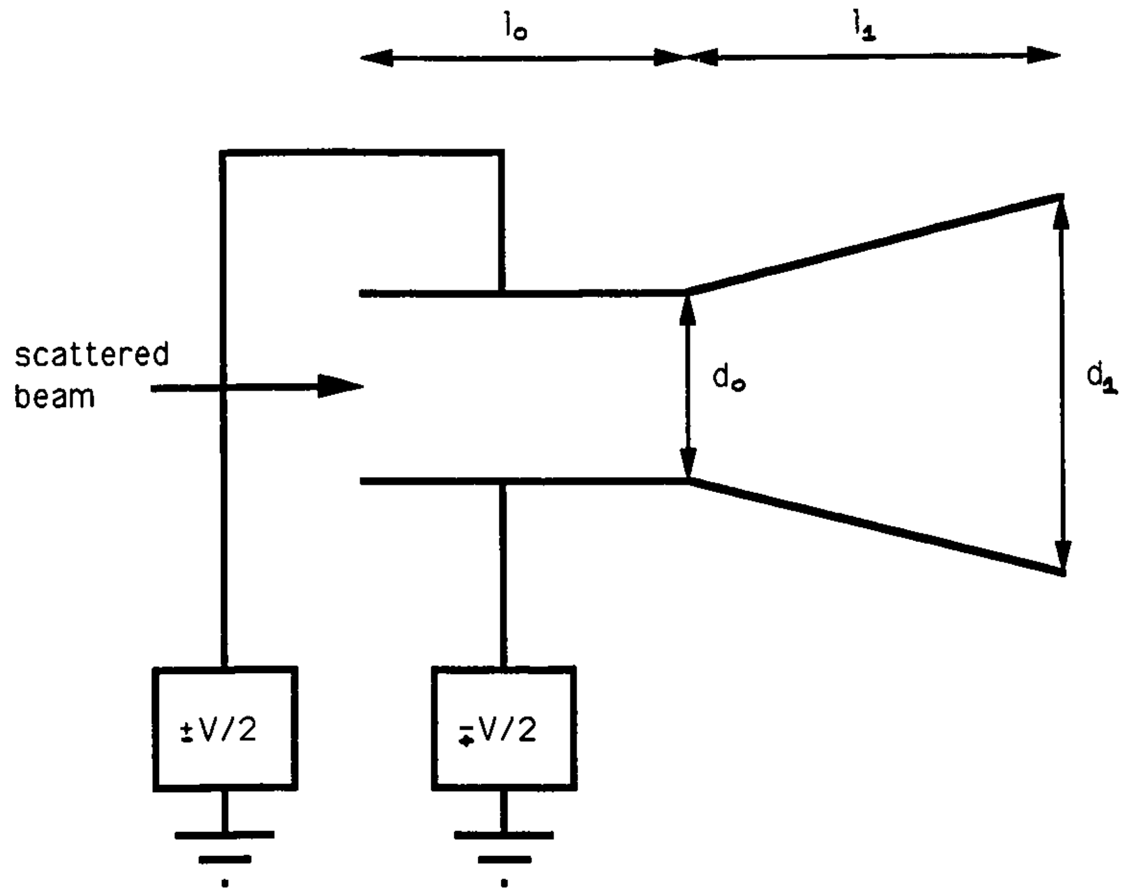

Figure 4.3

Deflectors

electrodes of length l_1 with a spacing d_0 at the entrance and d_1 at the exit, the angle of deflection is given by

$$\theta_{\text{non-par.}} = \frac{q}{2E} \frac{l_1}{d_1 - d_0} \ln\left(\frac{d_1}{d_0}\right) V \ . \tag{17}$$

For the combined parallel and tapered deflector configuration of the present surface physics system the angle of deflection θ is related to the voltage V across the electrodes by the following expression:

$$\theta = \frac{q}{2E}\left[\frac{l_0}{d_0} + \frac{l_1}{(d_1 - d_0)} \ln\left(\frac{d_1}{d_0}\right)\right] V \ . \tag{18}$$

The parameters d_0, d_1, l_0 and l_1 are the geometrical distances shown in figure 4.3. The numerical values are

$$d_0 = 1 \text{ cm}$$
$$d_1 = 2 \text{ cm}$$
$$l_0 = 2 \text{ cm}$$
$$l_1 = 2 \text{ cm} \ .$$

The angle of deflection needed for a beam to strike the top channeltron is $\theta = 21.8°$. The deflectors are designed to provide this deflection to an ion beam of $E = 10$ keV by applying a voltage $V = 2.25$ kV across the electrodes.

The energy resolution of a measurement can be determined by examining the effect of a small variation in energy ΔE on the deflection distance x defined in figure 4.4. For the sake of simplicity the case of parallel electrodes will be studied (equation (16)). For small angles

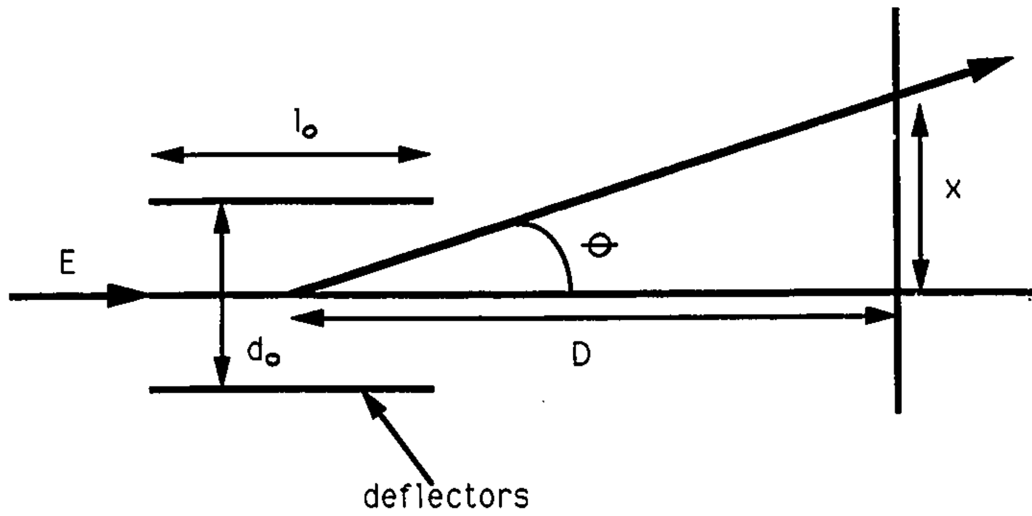

The ions appear to emerge from the centre of the electric field region.

Figure 4.4

Deflection Parameters

the angle of deflection θ can be expressed by the approximation

$$\theta \cong \frac{x}{D} . \tag{19}$$

It is easily deduced that a decrease of ΔE in ion energy will result in an increase of Δx of the deflection distance. Equations (16) and (19) can therefore be combined as follows:

$$\frac{x+\Delta x}{D} = \frac{q}{2(E-\Delta E)} \frac{l}{d} V \tag{20}$$

or

$$\frac{x+\Delta x}{D} = \frac{q}{2E\left(1-\frac{\Delta E}{E}\right)} \frac{l}{d} V . \tag{21}$$

Since ΔE is a small variation of the ion energy the approximation

$$\frac{1}{1-\frac{\Delta E}{E}} \cong 1+\frac{\Delta E}{E} \tag{22}$$

is valid. Substituting approximation (22) in equation (21), then using equations (16) and (19), we obtain

$$\frac{x+\Delta x}{D} = \frac{q}{2E} \left(1+\frac{\Delta E}{E}\right) \frac{l}{d} V , \tag{23}$$

and

$$\frac{\Delta x}{D} = \frac{q}{2E} \frac{\Delta E}{E} \frac{l}{d} V , \tag{24}$$

thus

$$\frac{\Delta x}{D} = \frac{x}{D}\frac{\Delta E}{E} , \tag{25}$$

finally

$$\frac{\Delta x}{x} = \frac{\Delta E}{E} . \tag{26}$$

The energy resolution of the surface physics system is calculated with the values $\Delta x = 1$ mm, which is the effective width of the rectangular channeltron aperture, and $x = 2$ cm, the position of the channeltron above beam height. Consequently the energy resolution $\frac{\Delta E}{E}$ is roughly 5%.

4.4 Detectors

As mentioned in section 4.1, the detection of the various particles scattered from the target surface is made by two channel electron multipliers (figure 4.5) located 7 cm downstream from the sample.

The circular aperture channeltron, located at the beam height, detects the neutral particles. The charged particles are deflected upward to the rectangular aperture channeltron, positioned 2 cm above the beam height. Depending on the polarity of the potential difference of the deflecting electrodes, this channeltron will detect either positives or negatives ions.

Each channel electron multiplier is linked to an independent pulse counting system. It consists of a pre-amplifier, an amplifier, a discriminator, a counter and a ratemeter (figure 4.6).

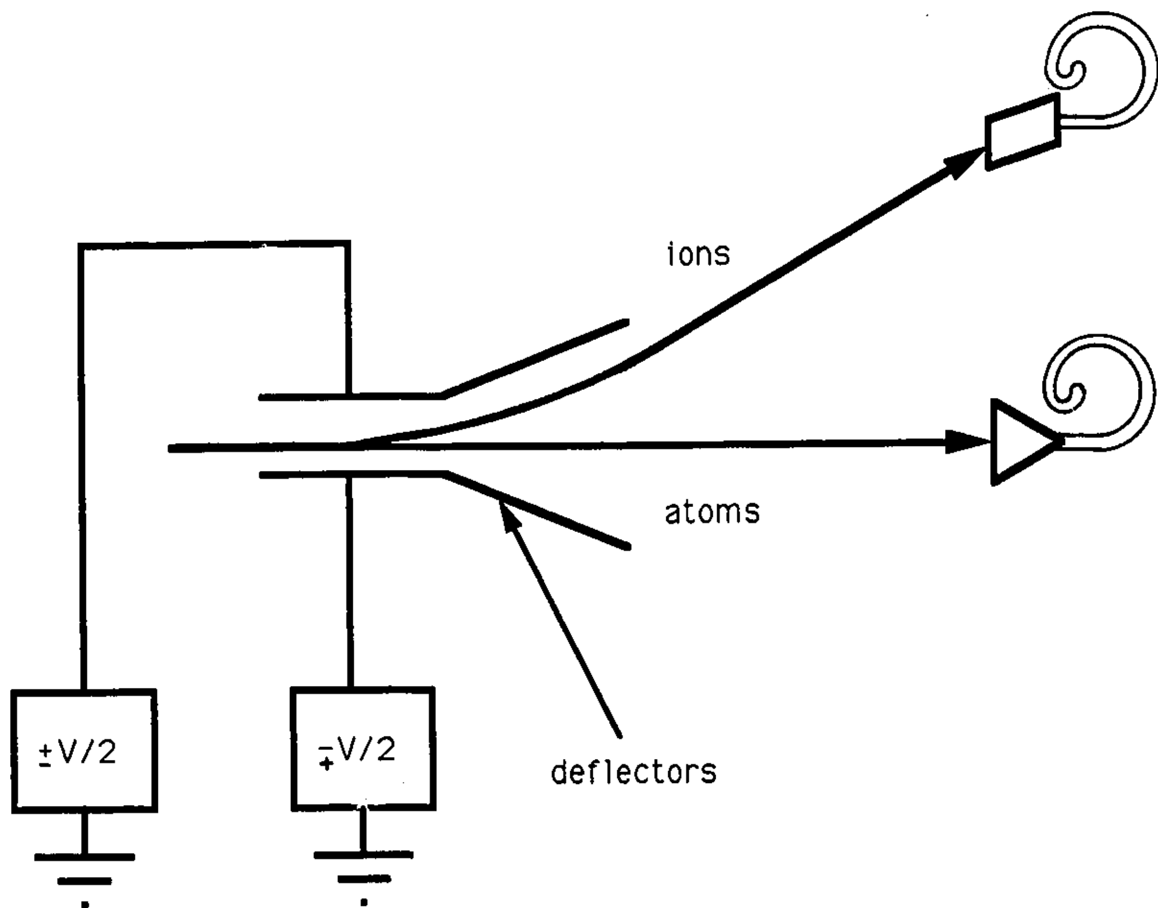

Figure 4.5

Channeltron Location

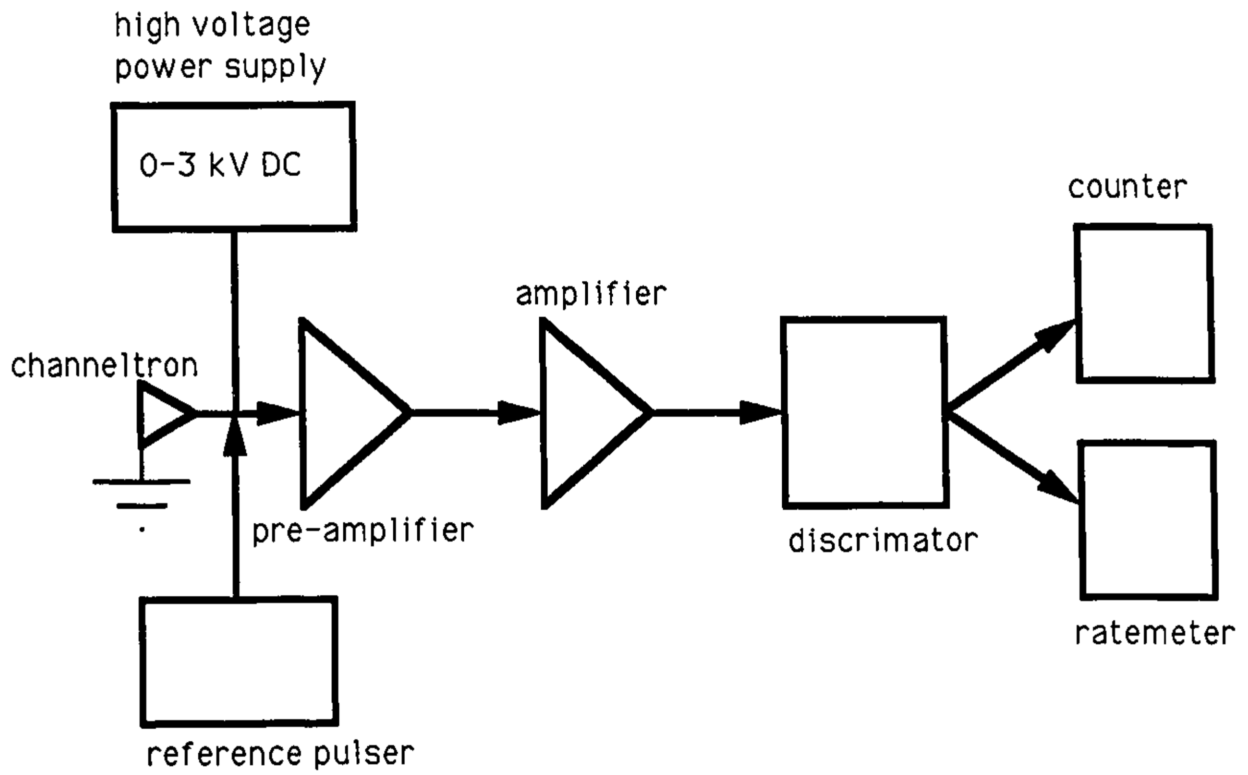

Figure 4.6

Pulse Counting System

CHAPTER 5 Proposed Measurement

The surface physics system is designed to directly provide plots of surface scattered particle counts versus deflecting voltage (figure 5.1).

The two digital signals from the channeltrons are converted to analogue signals in ratemeters and are then fed into a ratio circuit. The output of the circuit, a (ion counting rate)/(atom counting rate) ratio, is the Y input of an XY recorder. It is proposed to use the counting rate ratio rather than the neutral counting rate and the ion counting rate separately, because initial experience of the system shows that the ion beam intensity on the sample fluctuates all the time, so that absolute scattered ion intensities probably cannot be normalized in any consistent way. The ion beam inside the chamber is too small to be measured directly as a current on a picoammeter.

The X input of the XY recorder is the potential difference of the deflectors, proportionally scaled down by a very simple voltage divider circuit (figure 5.2).

From equation (18) it is clear that the deflecting voltage V is proportional to the scattered ion energy E, all other parameters d_0, d_1, l_0, l_1 and θ being kept constant. The X axis of a plot therefore represents the scattered ion energy. This horizontal scale can be calibrated with the

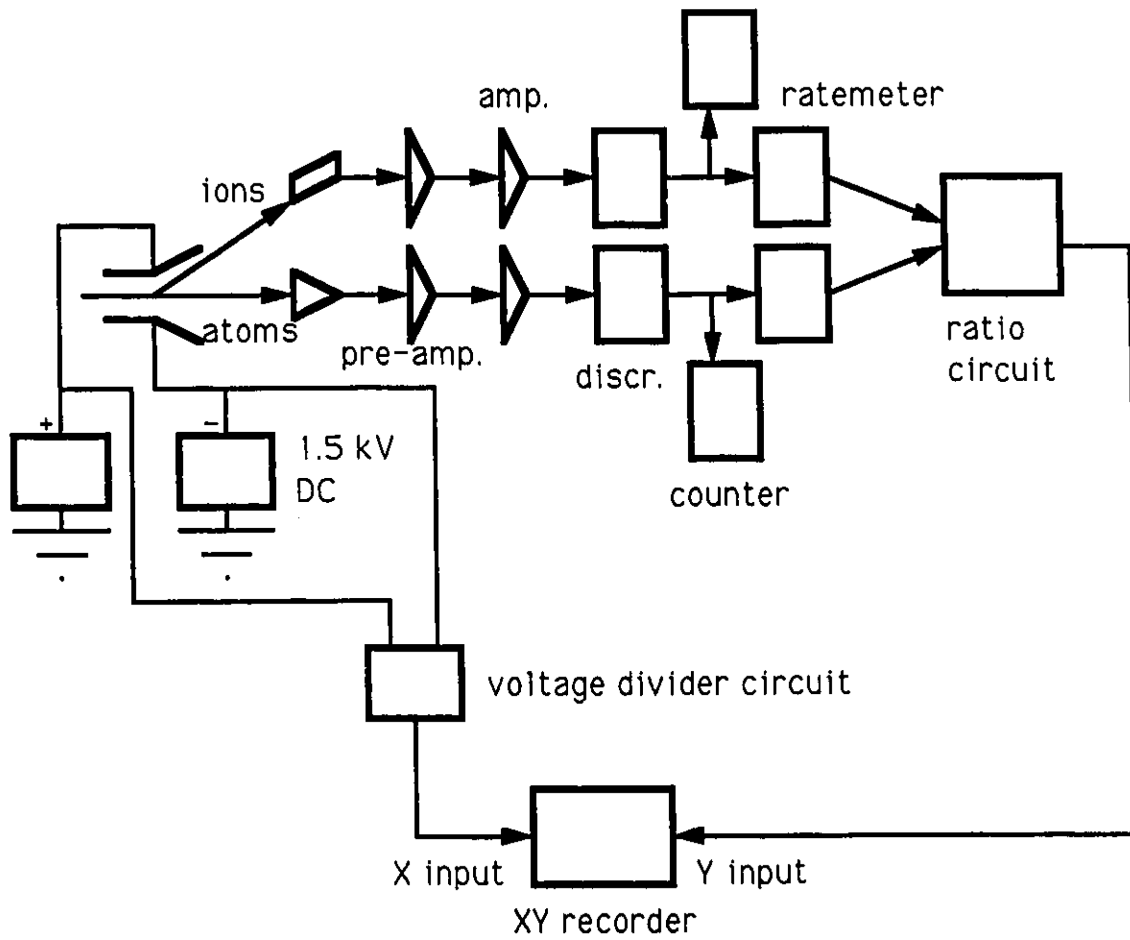

Figure 5.1

Complete Measurement System

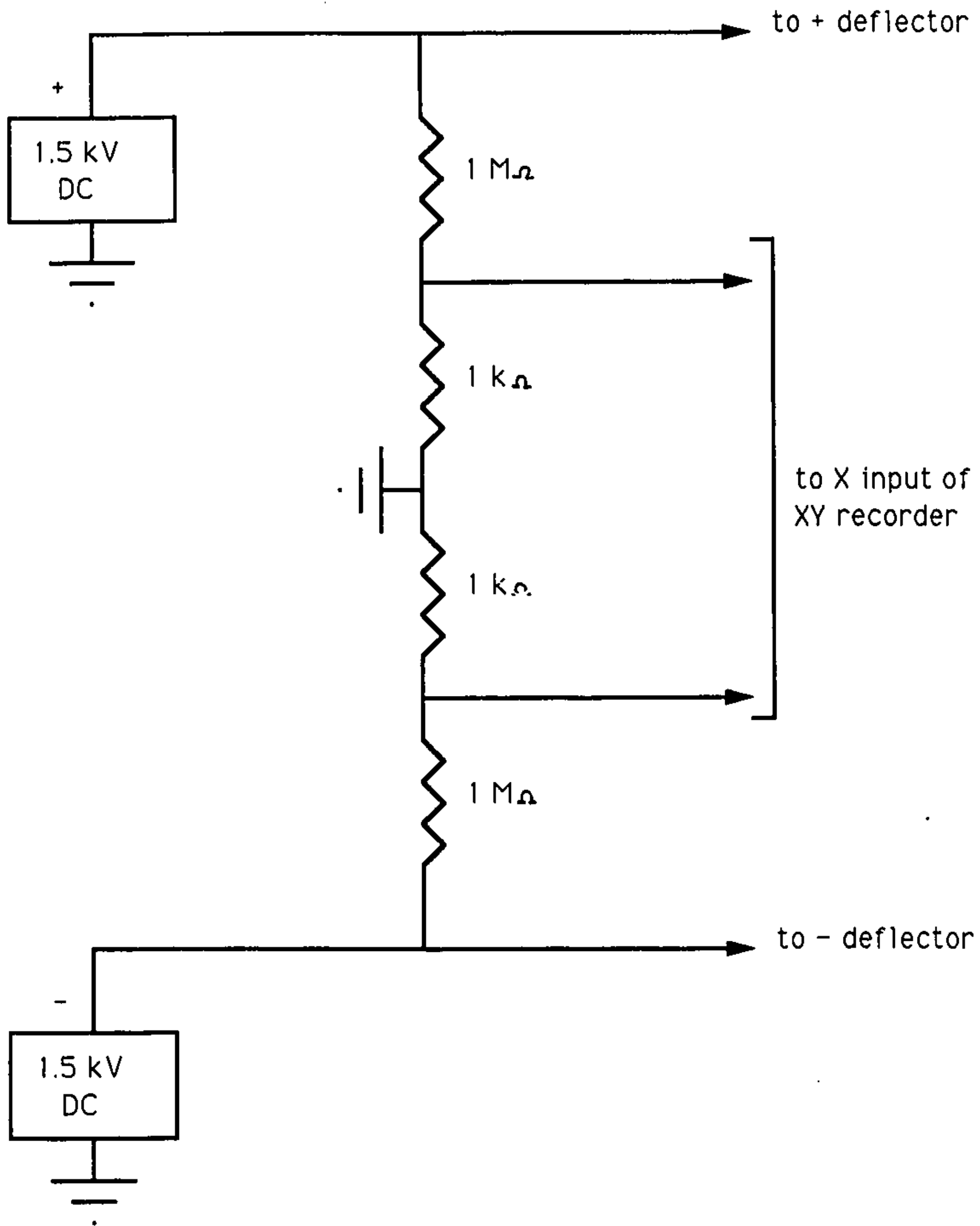

Figure 5.2

Voltage Divider Circuit

help of a known energy value, for example the value of the energy of the incident ion beam.

Each individual plot from the XY recorder will be a function of

- the incident ion beam:
  - element
  - electric charge
  - energy
  - angle with surface,
- the surface sample:
  - element
  - crystallographic direction
  - cleanliness
  - adsorbate coverage,
- the scattering angle.

It is proposed to combine a number of plots with the same incident ion beam and surface sample characteristics but recorded at different scattering angles (figure 5.3). Each resulting graph of the scattering angle ϕ (figure 5.4) versus the scattered ion energy E would be a collection of "equi-counting rate ratio" lines. In other words this contour representation will give the measured intensity (counting rate ratio) as a function of the final energy and the scattering angle. Experiments of this type have been performed[4].

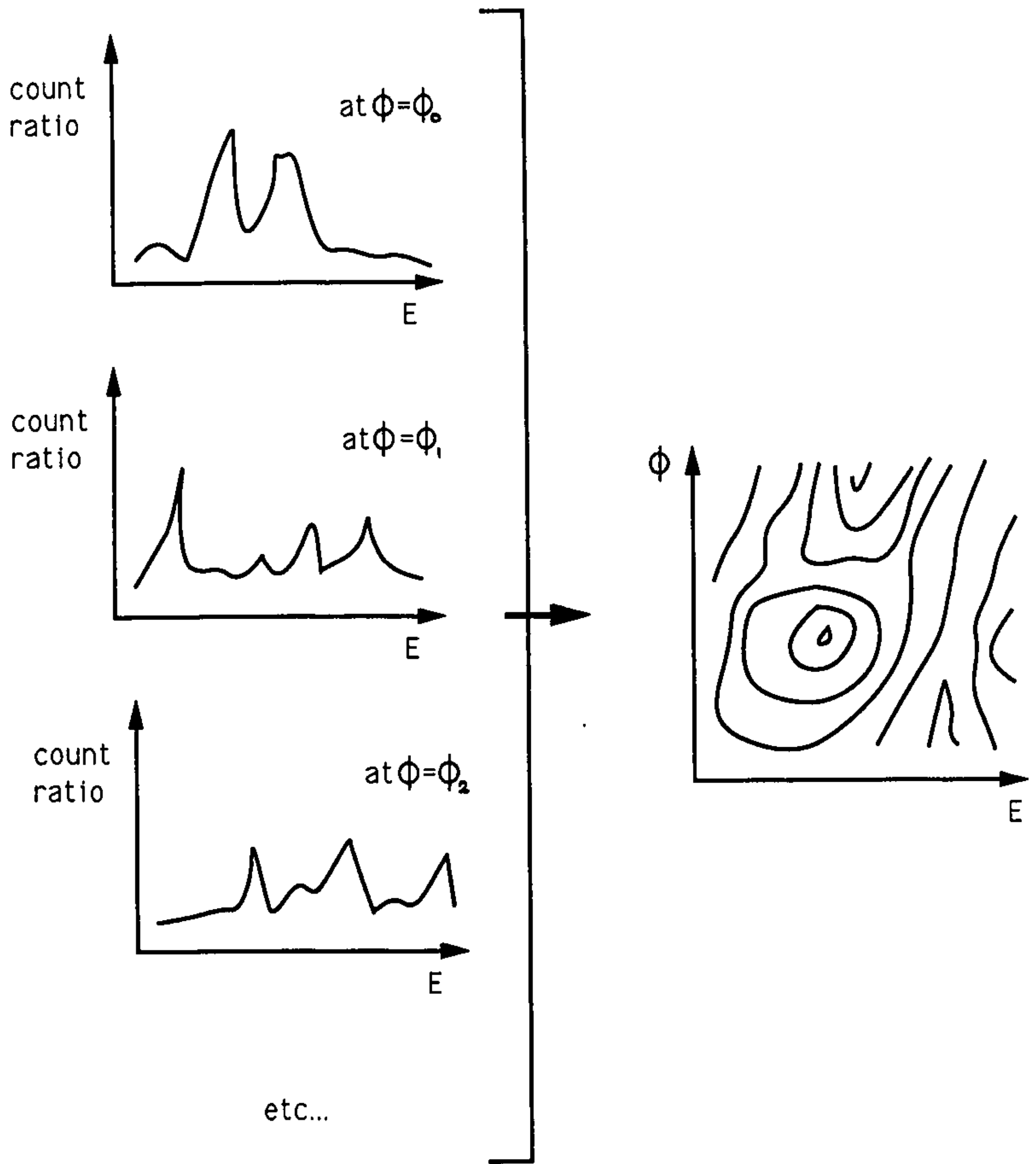

Figure 5.3

Example of Resulting Graphs

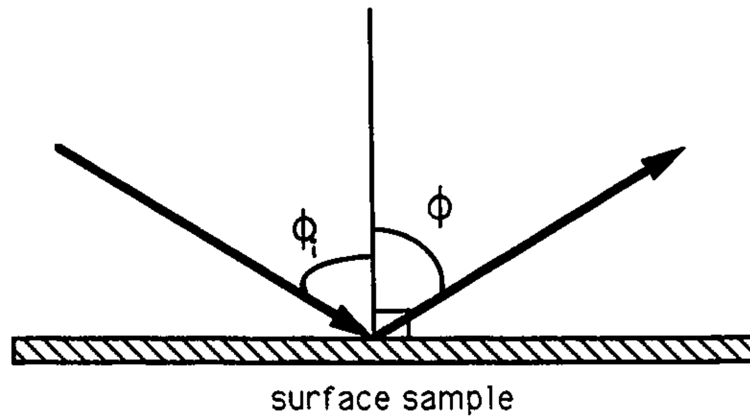

ϕ_i : incident angle

ϕ : scattering angle

Figure 5.4

Definition of the Scattering Angle

CHAPTER 6 Conclusion

The surface physics system is very close to being operational. The vacuum system is in working order and a considerable amount of experience in running it has been acquired. The arc discharge ion source, while it has produced beams of sufficient intensity, continually broke down and should be replaced with a R.F. type source. The other beamline components (accelerator, steerers and bending magnet) are ready for use. The commercially made sample manipulator, holder and electron beam heater, as well as the homemade electron beam heater power supply, have been installed and tested. The deflecting electrodes and the two channeltrons are in place in the main chamber on the rotating platform assembly with all connections ready. The detection electronics is also set up and working except for the ratio circuit still under development. A Si(100) surface sample is in the UHV main chamber but some mechanical alignment of the incident beam on the sample and of the scattered beam on the detectors needs to be done. Measurements are predicted for the near future.

Planned improvements to the system include the addition of an ion sputtering gun for further surface cleaning and of a High Energy Electron Diffraction (HEED) system for surface diagnostics. With the installation of a needle valve on the

main chamber section various surface coverages could be studied. An all-metal leak is already available for that purpose. An on-line computer data acquisition system would increase the speed of measurement making, facilitate the processing of data and improve the presentation of results.

The UHV surface physics system will make possible a variety of useful measurements on the surfaces of materials. It will allow the exploration of monolayers of surface structure and the determination of atom location on surfaces[5].

References

[1]C. Antonsen, *M.Sc. Thesis* (University of Ottawa, Ottawa, 1988).

[2]E. H. Kennard, *Kinetic Theory of Gases* (McGraw-Hill, New York, 1960).

[3]G. F. Weston, *Ultrahigh Vacuum Practice* (Butterworths, London, 1985).

[4]P. Haochang, T. C. M. Horn and A. W. Kleyn, *Harpooning in Scattering of* O_2^+ *from K-Ag*(111) (Journal of Electron Spectroscopy and Related Phenomena 45, 361-370, Amsterdam, 1987).

[5]J. F. Van Der Veen, *Ion Beam Crystallography of Surfaces and Interfaces* (Surface Science Reports 5, 199-288, Amsterdam, 1985).